Soils and Rocks
An International Journal of Geotechnical and Geoenvironmental Engineering
www.soilsandrocks.com
ISSN 1980-9743
ISSN-e 2675-5475

# Method for predicting the shear mechanical behavior of rockfill material

Tennison Freire de Souza Junior[1#], Sidnei Helder Cardoso Teixeira[2], Alessander Christopher Morales Kormann[1]

Case Study

**Keywords**
Rockfill
Large scale test
Friction angle

**Abstract**

Rock is a commonly utilized material in the construction of rockfill dams, protective ripraps for dam slopes, and stabilization of natural slopes. These materials demonstrate favorable performance under both static and dynamic loading conditions and are frequently more cost-effective compared to alternative stability solutions and construction methods for dams. The large dimensions and density of rock materials make it challenging to conduct representative mechanical tests and develop practical mathematical models that accurately describe their mechanical behavior at a real scale. This study proposes a hyperbolic prediction model for the shear mechanical behavior of earthfills, based on the outcomes of large-scale shear tests conducted on riprap samples with varying average dimensions ($D_{50}$). Analysis of the data revealed that the hyperbolic model exhibited good agreement with the graphs depicting shear box inclination mobilized friction angle θ (°) versus shear displacement $\delta$ (mm), in relation to the riprap diameter $D_{50}$. Moreover, the parameters α (Stiffness index) and β (Asymptotic index), along with the hyperbolic model, displayed a promising interrelationship of high quality.

## 1. Introduction

In general, rockfill is a composition of natural rocks of various dimensions arranged in a layer to serve specific purposes in geotechnical projects. According to Cruz et al. (2014), rockfills consist of large rock blocks with diameters ranging from 0.50 m to 1.0 or 2.0 m, and their mechanical strength is influenced by factors like mineralogy, granulometry, void ratios, shape, moisture content, grain compressive strength, size, texture, and time. The characteristics of rocks can be categorized into two main aspects: physical properties (including density, porosity, permeability, water absorption, hardness, and thermal conductivity) and mechanical properties (such as compressive, direct or indirect tensile, shear and impact resistances, deformability, elasticity, and abrasiveness) (Frascá, 2019).

These rocky materials are commonly utilized in civil engineering projects, including as rockfill for natural slopes (Maynord et al., 1989), gabion walls (Fracassi, 2017), dam slope protection, and coastal margin protection (Vick, 1990; Cruz et al., 2014; Sandroni & Guidicini, 2021; Rawee et al., 2022). Due to their density and weight, they demonstrate increased resistance to static loads and dynamic wave impacts, rendering them mechanically robust and long-lasting.

From a technical perspective, the slope inclination of a rock-filled embankment can serve as a contributing factor to failure. Hence, the configuration of the slope significantly influences the static stability of a dam or natural slopes. Moreover, the base of the slope is recognized as the most vulnerable component of the structure, highlighting the necessity for performing appropriate mechanical assessments.

The substantial geometric dimensions of these material particles render it unfeasible to conduct laboratory testing under controlled conditions. ASTM D4767-04 (ASTM, 2020a) and ASTM D7181 (ASTM, 2020b) stipulate that the grain diameter should be 1/6 of the specimen diameter to prevent scale effects in triaxial tests, whereas rockfill particle diameter typically exceeds several decimeters. Cruz et al. (2014) note that much of the information available in the literature has been derived from back-analysis in numerical models of rockfill dams with concrete facings. In dam structure analysis practice, the Leps graph (Leps,1970) is commonly utilized to estimate rockfill strength parameters. Nevertheless, these estimates are not based on measured data but are instead approximations.

[#]Corresponding author. E-mail address: tennisongeotec@gmail.com
[1]Universidade Federal do Paraná, Programa de Pós-graduação em Engenharia Civil, Curitiba, PR, Brasil.
[2]Universidade Federal do Paraná, Departamento de Engenharia da Civil, Curitiba, PR, Brasil.

Submitted on January 5, 2025; Final Acceptance on May 5, 2025; Discussion open until August 31, 2025.
Editor: Renato P. Cunha
https://doi.org/10.28927/SR.2025.000225

One method for testing these materials involves conducting large-scale direct shear tests, also known as tilt tests, as proposed by Barton & Kjaernsli (1981). This testing procedure mimics a shear test on a scale appropriate for assessing rockfill, while keeping the normal stress on the sample constant. The test yields data on the angle of failure based on the inclination angle of the box. Nevertheless, there is currently no numerical model available that can replicate the response of this test to simulate various scenarios involving rocks with intermediate $D_{50}$ values and their corresponding trends.

Hence, the objective of this article is to introduce a hyperbolic model for the mechanical characteristics of rockfills. This model enables the representation of the relationship between shear box inclination (θ in degrees) and displacement ($\delta$ in millimeters), facilitating the determination of the material's stiffness and its corresponding failure angle. This could be done since, similarly to stress-strain curves, displacement and mobilized friction angle shows a hyperbolic trend, especially due to the existence of an asymptotic limit value (the failure angle). At this stage, the rockfill reaches a constant shear stress as continuous displacement occurs, representing, from a mechanical standpoint, the full mobilization of friction and interlocking between particles.

## 2. Background

A recommendation suggests that the slope of the riprap should ideally have a ratio of 2:1 under standard conditions. However, a flatter slope may be deemed necessary based on the slope factor of safety, taking into account groundwater percolation or the potential occurrence of rapid drawdown. In situations where steeper slopes exceeding 2:1 are unavoidable, it is advisable to contemplate increasing the average size of the stones and the thickness of the riprap.

Additionally, the angularity of the rocks plays a crucial role; rocks with higher angularity exhibit a greater angle of repose. In cases where rounded stones are utilized, they should be positioned on relatively flat slopes (not surpassing 2.5:1), and the $D_{50}$ size should be augmented by 25%, along with an increase in the riprap thickness (USDA, 1989).

The optimal suggested gradation for riprap involves a continuous gradation curve, where $D_{max}$ equals 1.5 times $D_{50}$. The minimum diameter may range from 2.5 cm to 60% of $D_{50}$ (Sandroni & Guidicini, 2021). In terms of the riprap layer thickness, it is advised that the thickness falls within the range of 1.2 to 1.7 times $D_{50}$, with the possibility of greater thickness depending on $D_{50}$ (Sherard et al., 1963).

Geotechnical engineers often use Leps' chart (Leps, 1970) for estimating the friction angle of failure. However, as can be seen in Figure 1, this method is based on the estimation of the parameter using various data from studies on rocks with certain mineralogies, considering the quality of the rock and the confining stress. Nevertheless, it is very important to consider factors such as angularity, shape, degree of saturation, grain size, and even other mineralogies beyond those presented in the study. Besides that, as can be seen in Leps chart, the friction angle influenced by normal stresses. As normal stress increases, the friction angle decreases. Particles breakage at contact can be an explanation for this observation.

Cruz & Nieble (1970) and Midea (1973) conducted research on modified basaltic and gneissic rockfill materials. They determined the strength characteristics through direct shear tests (DS) using boxes of dimensions 20 cm × 20 cm × 20 cm and 100 cm × 100 cm × 40 cm, as well as triaxial tests (TR) on specimens with a height of 10 cm. Midea (1973) reported a decrease in the friction angle of gneiss samples with an increase in fine content. Cruz & Nieble (1970) found that

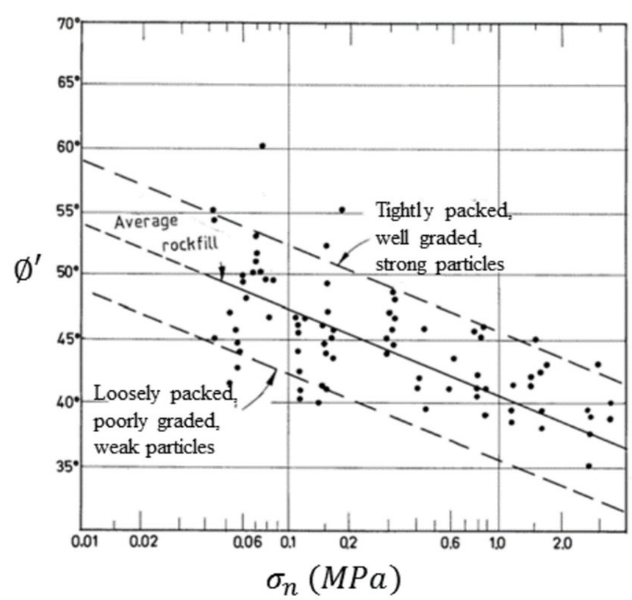


**Figure 1.** Empirical correlation between the angle of repose vs confining pressure (Leps, 1970).

cycled basalt samples exhibited a reduction of approximately 20%. These findings are summarized in Table 1 below.

Terzaghi (1960) conducted mechanical tests on dry rocks, wet rocks, and saturated rocks. The study concluded that water does not act as a lubricant in rock contacts, leading to similar friction angles in wet and saturated rock masses. However, the presence of water weakens the rock, increasing deformation due to particle breakage and crushing. Additionally, the strength of the blocks is influenced by stress levels, akin to soils in general, and by progressive fracturing, resulting in a reduction of the friction angle. Ultimately, the study demonstrated that rock masses containing angular blocks exhibit greater deformability compared to those with rounded blocks.

However, research on triaxial and direct shear tests carried out on basalt earth fill samples from Marimbondo Dam in Brazil has shown that the shear strength is positively correlated with relative density and negatively correlated with the degree of material weathering. Results from accelerated weathering tests have indicated that the rate of strength reduction due to weathering diminishes over time. Additionally, the strength envelope converges towards a lower limit, representing the fully weathered material (Sayão et al., 2005).

The four primary types of riprap failure identified in the literature are particle erosion, translational sliding, modified slumping, and slumping (Blodgett, 1986). Particle erosion is characterized by the displacement of rock blocks and is typically associated with the use of undersized rocks, impact from debris, or direct flow impingement. Translational sliding, which involves the failure of the revetment parallel to the side slope, is often caused by toe scour and a decrease in the support capacity along the base of the revetment. Modified slumping, where the blanket shifts without toe failure, is commonly triggered by excessively steep slopes. Slumping, a rotational failure, typically occurs on high banks due to the static instability of the protected slopes.

Rock riprap offers erosion resistance by utilizing a blend of stone size and weight, stone durability, and the gradation and thickness of the riprap blanket. The interlocking of angular rocks enhances resistance to the displacement of individual blocks within the revetment. In channel structures, the stability of riprap protections is notably influenced by stream characteristics, as the sizing is interconnected with flow velocity, rock dimensions, and channel dimensions (such as the slope of the banks, slope of the bed, and area) (Fracassi, 2017).

**Table 1.** Type of altered rocks and parameters (Cruz et al., 2014).

| Material | Test | $D_{max}$ (mm) | $\varphi^1$(°)* | Ref. |
|---|---|---|---|---|
| Compact crystalline basalt (A) in nature | DS | 80 | 53 | Cruz & Nieble (1970) |
| | DS | 50 | | |
| | TR | 25 | | |
| Vesicular and Amygdaloidal Basalt (sample 1) | DS | 80 | 52 | Cruz & Nieble (1970) |
| | TR | 40 | | |
| | | 25 | | |
| Vesicular and Amygdaloidal Basalt in natura | DS | 80 | 55 | Cruz & Nieble (1970) |
| | TR | 40 | | |
| | | 25 | | |
| Vesicular and amygdaloidal basalt (sample 2) cycled | DS | 80 | 44 | Cruz & Nieble (1970) |
| | TR | 40 | | |
| | | 25 | | |
| Vesicular and amygdaloidal basalt (sample 3) cycled | DS | 80 | 43 | Cruz & Nieble (1970) |
| | | 40 | | |
| | TR | 25 | | |
| Gneiss with 3% to 9% fines | DS | 50 | 50 | Midea (1973) |
| Gneiss with 26% to 49% fines | DS | 5 | 47 | Midea (1973) |
| Gneiss with 100% fines | DS | - | 40 | Midea (1973) |

*Friction angle to $\sigma$ = 1 kgf/cm² (°).

## 3. Methodology

The proposed methodology for obtaining the results is based on real-scale studies considering the granulometric variation of tinguaite riprap. The entire executive procedure of the experimental tests is described below.

### 3.1 Rockfill material

The rockfill material utilized underwent laboratory characterization based on physical and mechanical criteria. The rock was identified as Tinguaite, a type commonly found in the southeastern region of Brazil. Tinguaite is described as a medium- to coarse-grained, unsaturated igneous rock consisting of essential alkali feldspar, nepheline, and aegirine, with or without sodium amphibole or biotite. Tinguaite is considered the hypabyssal equivalent of phonolite (Allaby, 2008).

The rockfill blocks were divided into samples of various diameters. The sample consisting of small blocks ($D_{50}$ = 150 mm) is indicative of the transition material located at the base of the dam (refer to Figure 2a). On the other hand, the samples containing medium and large blocks ($D_{50}$ = 400 mm and $D_{50}$ = 600 mm, respectively) represent the material forming the upstream and downstream slopes of the dam (Figure 2b). This material is classified as grading E, which is characteristic of a densely graded zone (DNIT, 2012).

Unconfined compression tests were conducted on tinguaite samples in saturated and unsaturated conditions based on ASTM D7012 (ASTM, 2014). The available tests also show that the altered material exhibits greater sensitivity in terms of strength when in saturated conditions. Additionally, the variability in block rupture stress may be related to the variability in the degree of weathering of the rockfill and the mineralogy of the blocks.

As can be seen in Table 2, depending on the condition of alteration and saturation of the rock, the average compressive stresses can vary. The more natural and intact the rock, the higher the ($\sigma_{cm}$ =72.82 MPa). However the more saturated and altered the rock, the lower the value of the compressive stress ($\sigma_{cm}$ =23.05 MPa). It is noted that the material has mechanical strength with a heterogeneous distribution (CV>10%).

It was found that the studied rockfill blocks exhibited a water absorption capacity exceeding 0.5% (refer to Table 3), a factor that contributes to the acceleration of the material

(a) (b)

**Figure 2.** Grain size distribution of the rip rap: (a) $D_{50}$ = 150 mm; (b) $D_{50}$ = 600 mm.

**Table 2.** Compressive strength of the rockfill material.

| Type | Condition | Samples | $\sigma_c$ (MPa) | $\sigma_{cm}$ (MPa) | $\Delta c$ (MPa) | $CV$ % |
|---|---|---|---|---|---|---|
| Tinguaite intact | Natural | 1 | 53.9 | 72.83 | 17.43 | 24% |
| | | 2 | 88.2 | | | |
| | | 3 | 76.4 | | | |
| | Saturated | 4 | 80.4 | 54.30 | 35.48 | 65% |
| | | 5* | 13.9 | | | |
| | | 6 | 68.6 | | | |

*With a pre-existing fracture.

**Table 3.** Characterization of rockfill material.

| Samples | Shape index | Dry unit weight (kN/m$^3$) | Bulk density (kN/m$^3$) | Water absorption (%) | Wear (%) |
|---|---|---|---|---|---|
| BR-PI-05 | 2.24 | 22.624 | 25.076 | 4.24 | 20.1 |
| BR-PI-06 | 2.24 | 22.536 | 24.928 | 4.18 | 21.6 |

**Table 4.** Los Angeles Abrasion tests on rockfill samples data.

| Sieve (mm) | | Mass (g) | BR-PI-05 | | BR-PI-06 | |
|---|---|---|---|---|---|---|
| | | | Retained mass (g) | Mass loss (%) | Retained mass (g) | Mass loss (%) |
| Coarse range | 60.3 - 50.0 | 1500 | 1463.80 | 2.41 | 1462.40 | 2.51 |
| | 50.0 - 38.0 | 1500 | 1492.20 | 0.52 | 1487.30 | 0.85 |
| | 38.0 -25.0 | 1005 | 980.40 | 2.45 | 983.53 | 2.14 |
| | 25.0 - 19.0 | 495 | 442.97 | 10.51 | 440.20 | 11.07 |
| | 19.0 -12.7 | 670 | 596.70 | 10.94 | 571.05 | 14.77 |
| | 12.7 - 9.5 | 330 | 251.07 | 23.92 | 268.99 | 18.49 |
| Fine range | 9.5 - 4.8 | 110 | 107.66 | 2.13 | 107.66 | 2.13 |
| | 4.8 - 2.4 | 110 | 108.00 | 1.82 | 108.00 | 1.82 |
| | 2.4 -1.2 | 110 | 102.90 | 6.45 | 102.90 | 6.45 |
| | 1.2 - 0.6 | 110 | 106.20 | 3.45 | 106.20 | 3.45 |
| | 0.6 - 0.3 | 110 | 103.00 | 6.36 | 103.00 | 6.36 |

weathering process (Pichler, 1942). Regarding the material's resistance to degradation on Los Angeles Machina, only particles with a grain size between 12.7 mm and 9.5 mm showed a mass loss exceeding 18% (see Table 4), which is characterized as "desirable" for rockfill structure construction (Yoshida, 1972). The tests were performed by ASTM C535 (ASTM, 2016) and ASTM C131 (ASTM, 2006).

### 3.2 Large-scale shear test

The procedure for the large-scale shear test closely followed the methodology proposed by Barton & Kjaernsli (1981). Due to the large size of the rock blocks, the density of the rockfill was not measured directly. Instead, it was controlled by gently placing the blocks into the box without the use of vibrations. This test aimed to assess the roughness of rock joints, specifically the Joint Roughness Coefficient (JRC), without the necessity of parallel grading curves. The test procedure was structured into four main stages. Initially, the apparatus was assembled, comprising two semi-boxes measuring 1.00 m × 2.00 m × 5.00 m (height × length × width). The test was conducted at a lifting rate of approximately 10°/min.

The semi-boxes were overlapped with a 5 cm spacing between them, as illustrated in Figure 3a. This spacing was maintained by screws on the sides, which were subsequently removed before the test. Markings on the external walls of the semi-boxes were used to monitor the displacement between the upper and lower sections during lifting. An angle gauge with a magnetic base was employed for angle measurements, while photographs taken orthogonally to the box's surface were utilized for displacement readings (refer to Figure 3b).

The second stage involves filling the container with the rockfill sample (refer to Figure 4). Backfilling was executed using a backhoe, where the material was directly deposited by the scoop of the equipment. Three different material samples were examined, differing in the averge diameter of the blocks. The samples tested had $D_{50}$ values of 150 mm, 400 mm, and 600 mm, categorized as small, medium, and large-sized blocks, respectively.

The third step involves removing the screws that secure the boxes and commencing the process of lifting the apparatus using a crane. During this step, measurements of the displacement between the boxes and their corresponding inclination angles are taken (refer to Figure 5a). Subsequently, the angle leading to the sample's rupture is identified (refer to Figure 5b).

### 3.3 Hyperbolic model proposed

The stress-strain response of soil is influenced by a multitude of factors, encompassing density, moisture content, composition, drainage characteristics, deformation conditions (e.g., plane strain or triaxial), loading duration, stress background, confining pressure, and shear stress (Duncan & Chang, 1970).

Initially, the hyperbolic model was developed to replicate the behavior of natural clays (Kondner & Horner, 1965;


(a) (b)

**Figure 3.** Equipment used in the test: (a) crane and the assembled artifact; (b) displacement and angulation measuring.


(a) (b)

**Figure 4.** Filling the shear box with the rockfill material: (a) filling in progress; (b) filling completed.

Kondner, 1963) and natural sands (Kondner & Zelasko, 1963). This model is applicable for analyzing both drained and undrained soils. Kondner's research suggested that the correlation between deviator stress and axial strain follows a hyperbolic curve that can be defined by specific parameters. By establishing an analogy with the approach proposed by Duncan & Chang (1970) for a direct shear condition, it is possible to describe it through Equation 1. The definition of symbols used on equations can be found on the List of symbols and abbreviations.

$$\tau = \frac{\varepsilon_s}{\alpha + \beta \varepsilon_s} \tag{1}$$

The partial derivative of the shear stress concerning shear strain in the elastic stage ( $\varepsilon_s = 0$ ) yields Equation 2:

(a) (b)

**Figure 5.** Large scale shear test: (a) during test; (b) final test.

$$\frac{\partial(\tau)}{\partial\varepsilon_s} = \frac{1}{\alpha + \beta\varepsilon_s} - \frac{\beta\varepsilon_s}{(a + \beta\varepsilon_s)^2} = \frac{1}{\alpha} \quad (2)$$

The limit of the shear stress for infinite axial deformation (plastic stage) is equivalently equal to $\frac{1}{\beta}$ (see Equation 3):

$$\lim_{\varepsilon_a \to \infty} (\tau) = \frac{\varepsilon_s}{\alpha + \beta\varepsilon_s} = \frac{1}{\beta} \quad (3)$$

In the direct shear test, the ultimate shear stress is related to the friction angle at failure (see Equation 4):

$$\varphi_f = \int(\tau) \quad (4)$$

During the test, the rotation of the box allows gravitational forces to mobilize the sliding of the rockfill. In this moment, the contact friction and interlocking of the rockfill create resisting forces. Under the limit equilibrium condition, where the rockfill ( $c'$ = 0) is in imminent failure (FS=1) based on Equation 5 and 6 (Coulomb, 1776). Therefore, when θ > $\varphi_f$, the box reaches an unstable condition (failure), but when θ < $\varphi_f$, the box is in a stable condition. At the same time, in the large-scale shear test, there is an approximate relationship between the final box inclination and the rock's friction angle at failure.

$$FS = \frac{\tan\theta_{\text{final}}}{\tan\varphi_f} \rightarrow 1 = \frac{\tan\theta_{\text{final}}}{\tan\varphi_f} \rightarrow \tan\theta_{\text{final}} = \tan\varphi_f \quad (5)$$

So,

$$\varphi_f = \theta_{\text{final}} \quad (6)$$

According to Duncan & Chang (1970), by plotting the stress-strain data using the hyperbolic model, it is simple to determine the values of the parameters α and β corresponding to the best-fit hyperbolic curve and the test data. Generally, the asymptotic value, represented by the ultimate deviator stress, is slightly greater than the shear strength, since the hyperbola remains below the asymptote at all finite strain values. Therefore, the hyperbolic model can be adapted to a relationship with the shear box inclination angle based on Equation 7. The mobilized friction angle during the test can be considered equal to the shear box inclination.

$$\theta = \frac{\delta}{\alpha + \beta\delta} \quad (7)$$

The α parameter influences the relationship between the box inclinations and low shear displacements. The β parameter directly influences the failure inclination (high shear displacements) of the box and, therefore, the failure friction angle ( $\varphi_f$ ).

Figure 6 illustrates the proposed hyperbolic model with its respective parameters α and β. Through this graph, it is possible to observe the non linear correlation between $\varphi_f$ and δ and the best fit of the calibration parameters. Ultimately, the model allows the normalization of the behavior between the rupture angle and the displacement according to Equation 8:

$$\frac{\theta}{\varphi_f} = \frac{\frac{\delta}{\delta_{\max}}}{a_n + \beta_n \frac{\delta}{\delta_{\max}}} \quad (8)$$

## 4. Results and discussions

In Figure 7, it can be observed that the experimental data for the box inclination vs. displacement relationship showed a hyperbolic trend regardless of the $D_{50}$ value, such that the proposed hyperbolic mathematical model accurately described the large-scale shear test results. The inclination angle of the box is equal to the friction

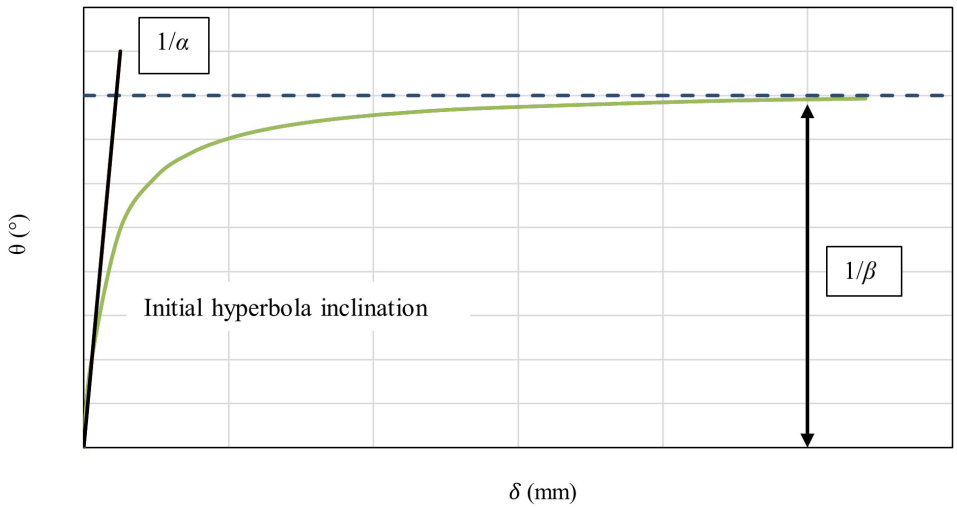


**Figure 6.** Hyperbolic model proposed.

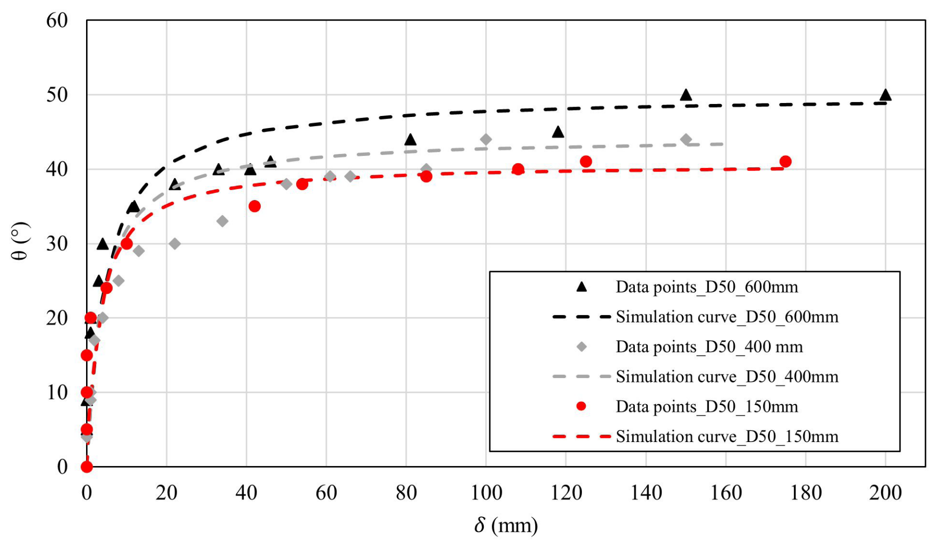


**Figure 7.** Relationship between the riprap's angle of repose and displacement in the shear plane.

angle mobilized during the test until reaching the failure condition, which is related to the constancy of the angle at large displacements.

It can be stated that as the $D_{50}$ value increased, the angle of failure also increased. This behavior relates to the weight-to-density ratio of the rockfill blocks, such that a higher ratio tends to result in greater inertia caused by shear strength (friction between the rocks).

Figure 8 perfectly illustrates the relationship between $D_{50}$ and $\varphi_f$. An excellent linear correlation between these parameters can be observed, characterized by $R^2 = 0.94$. Equation 9 mathematically reproduces this relationship:

$$\varphi_f\left(^\circ\right) = 0.0197 D_{50} + 3.459 \tag{9}$$

Finally, when evaluating the values of parameters α (mm/°) and 1/β (°), it was observed that there is a linear correlation between them as a function of $D_{50}$ (see Figure 9). Therefore, it is possible to simulate θ vs δ curves for intermediate values, and thus, it would be possible to estimate possible displacements as well as other failure angles. Equation 10 describes the linear correlation with excellent quality ($R^2 = 0.962$):

$$\alpha = 0.0101\left(\frac{1}{\beta}\right) + 0.0479 \tag{10}$$

As can be seen in Figure 10, it was possible to normalize the behavior of the curves using Equation 11. From the calibration of the $a_n = 0.03$ and $\beta_n = 1$ parameters, the test responses were normalized relative to the maximum rupture values. The curve was able to present the response of

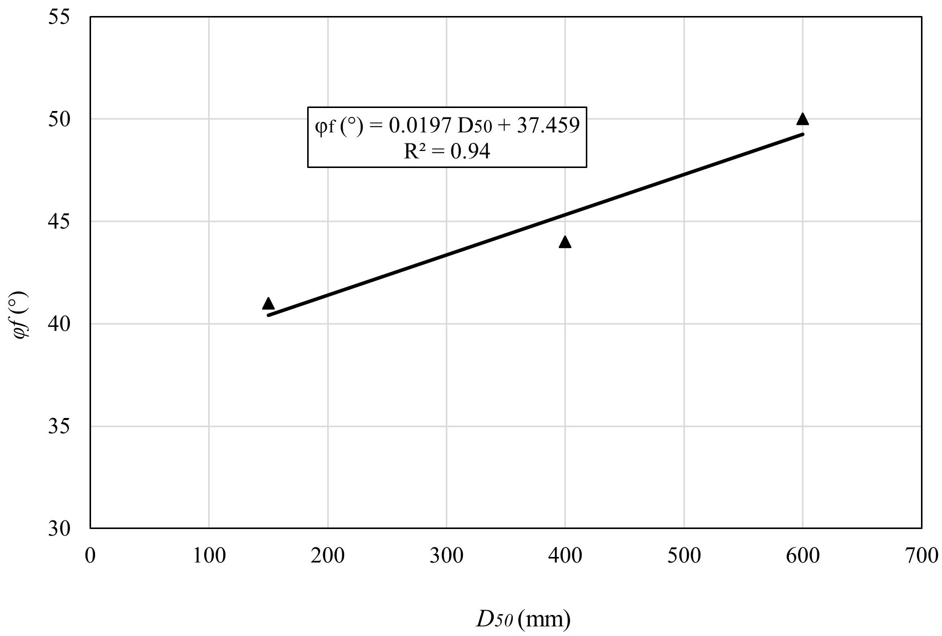


**Figure 8.** Relationship between the riprap's angle of repose and average diameter of the riprap.

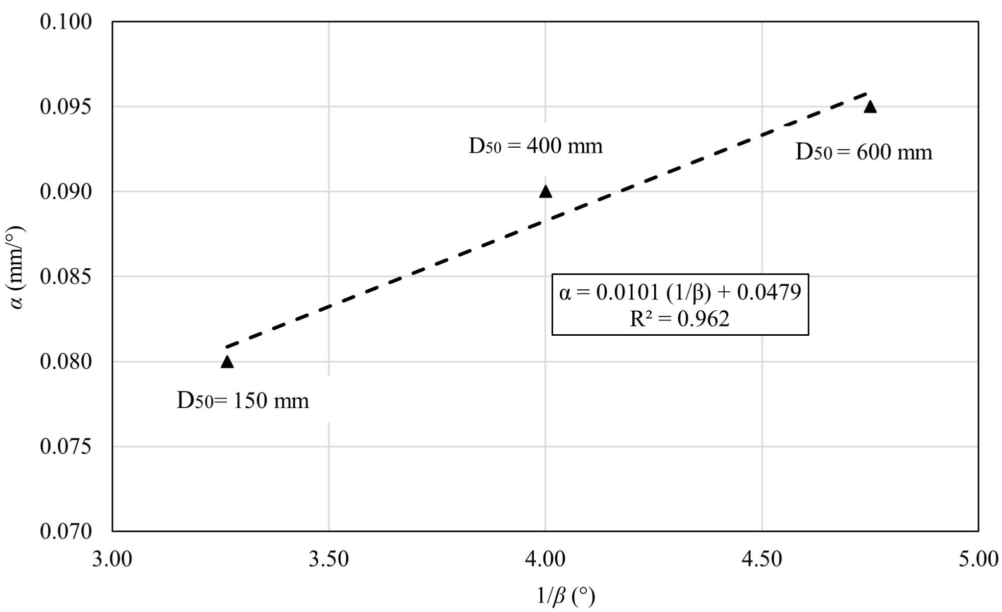


**Figure 9.** Relationship between calibration parameters of the hyperbolic model.

different rock samples with different $D_{50}$ with low dispersion and simplicity, making it suitable for estimating rocks with intermediate dimensions but with similar characteristics and properties (density, shape factor, mineralogy, etc.).

$$\frac{\theta}{\varphi_f} = \frac{\dfrac{\delta}{\delta_{\max}}}{0.03 + 1\dfrac{\delta}{\delta_{\max}}} \tag{11}$$

The analysis of the curves presented, especially in Figures 7 to 10, provides a clearer understanding of the influence of the α and β parameters on the mechanical behavior of the rockfill. The α parameter is associated with the initial stiffness of the material, affecting the slope of the curve at small displacements, while the β parameter governs the behavior at large deformations and is directly related to the failure angle. By comparing Figure 8 and Figure 9, it can be seen that as the α parameter increases,

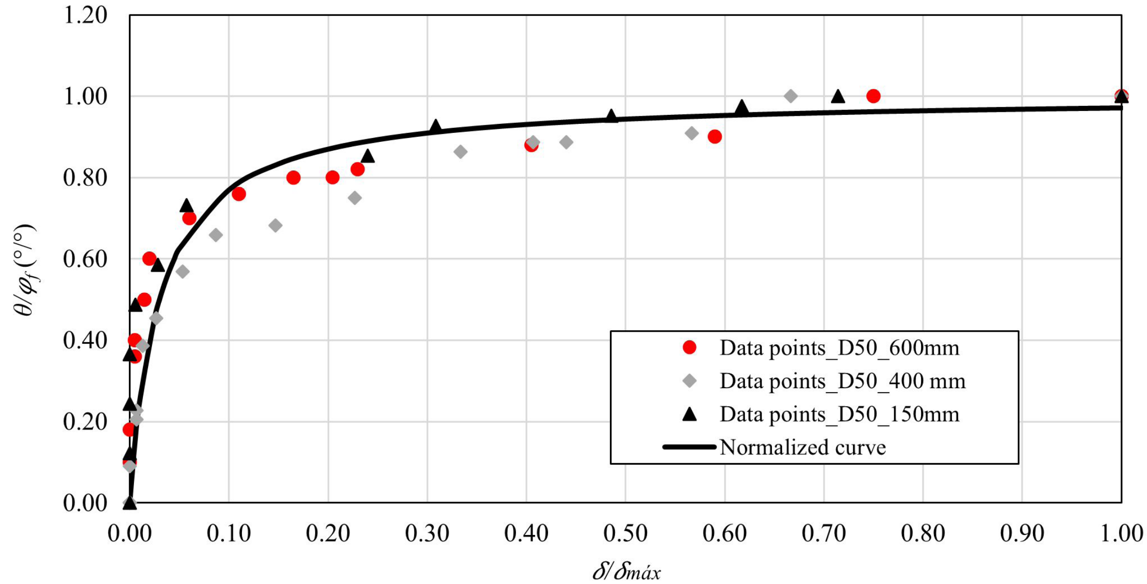


**Figure 10.** Normalization curve of the mechanical behavior of rockfills.

the value of 1/β (Equation 10) increases. This trend is also associated with $D_{50}$ and friction angle.

The hyperbolic shape of the curves reflects the gradual transition from the initial elastic regime to the failure state, accurately characterizing the material's nonlinear behavior. Furthermore, the variation in $D_{50}$ proved to be a determining factor in the overall performance of the rockfill: samples with higher $D_{50}$ values exhibited greater failure angles, which can be attributed to the increased inertia and internal friction between the blocks due to their greater mass and interlocking. These observations have direct practical implications for the design of rockfills, suggesting that controlling $D_{50}$ can be an effective strategy to optimize the stability of slopes and rockfill-based structures.

## 5. Conclusions

This article presents a method for estimating the angle of shear rupture through large-scale shear tests on tinguaite rockfill. During the research, it was observed that the hyperbolic model was able to accurately reproduce the variation in box rotation relative to relative displacement with excellent adherence, and it was also possible to normalize the behavior using a single hyperbole. Regarding the behavior of the proposed model, some aspects can be stated below:

- The hyperbolic model effectively and concisely replicated the mechanical response of the rockfill in tilt tests. The suggested mathematical model demonstrated a strong correlation with the experimental findings of the θ (°) vs $\delta$ (mm) relationship derived from the extensive shear tests introduced by Barton & Kjaernsli (1981);
- The relationship between the failure friction angle ($\varphi_f$) in degrees and mean stone size of the rockfill ($D_{50}$) was found to be linear. Specifically, as the value of $D_{50}$ increased, the angle of failure also increased;
- The parameters α and β, when appropriately calibrated, exhibited a linear relationship among themselves and with the $D_{50}$ value. A decrease in the $D_{50}$ value corresponded to a increase in the α value and an increase in the value of 1/β;
- Through the proposed hyperbolic model, it is feasible to replicate the mechanical response of rockfill particles of intermediate sizes, given that the parameters α and β are appropriately calibrated;
- Upon assessment of the tests, the test results were normalized according to the ratio $\delta/\delta_{máx}$;
- This research was conducted based on a limited number of tests and unique normal stress. Although relevant conclusions were found, they may be limited and could differ for other untested materials and normal stresses.

## Acknowledgements

The authors acknowledge the support of CNPQ (National Council for Scientific and Technological Development) and CAPES (Coordination for the Improvement of Higher Education Personnel) for funding research in Brazil.

## Declaration of interest

The authors declare that they have no known competing financial interests or personal relationships that could have appeared to influence the work reported in this paper.

## Authors' contributions

Tennison Freire de Souza Junior: conceptualization, methodology and writing - original draft preparation. Sidnei Helder Cardoso Teixeira: investigation, data curation, reviewing and validation. Alessander Christopher Morales Kormann: writing - reviewing and editing.

## Data availability

The data supporting the analyses and results of this study are available from the corresponding author upon request and as needed.

## Declaration of use of generative artificial intelligence

This work was prepared without the assistance of any generative artificial intelligence (GenAI) tools or services. All aspects of the manuscript were developed solely by the authors, who take full responsibility for the content of this publication.

## List of symbols and abbreviations

$\alpha$ Stiffness index (mm/°);
$\beta$ Asymptotic index ( $^{\circ -1}$ );
$\alpha_n$ Normalized Stiffness index;
$\beta_n$ Normalized Asymptotic index;
$\gamma$ Specific weight of the rock (kN/m$^3$);
$\Delta c$ Standard deviation;
$\delta$ displacement (mm);
$\delta_{max}$ Max. displacement (mm);
$\varepsilon_s$ Shear deformation (%);
$\theta$ Rotation box angle (°);
$\theta_{final}$ Final Rotation box angle (°);
$\varphi_f$ Failure friction angle (°);
$\varphi^1$ Friction angle to $\sigma$ = 1 kgf/cm$^2$ (°);
$\sigma_c$ Compressive strength (MPa);
$\sigma_{cm}$ Mean compressive strength (MPa);
$\sigma_n$ Normal stress (kPa);
$\tau$ Shear stress (kPa);
CV Variation coefficient;
$c'$ Cohesion intercept (kPa);
$Z$ Height of the half-box (m);
$D_{50}$ Mean stone size (mm);
$D_{\text{máx}}$ Maximum diameter (mm);
DS Direct shear test;
TR Triaxial compression test;
JRC Joint Roughness Coefficient.

## References


Allaby, M. (2008). *A dictionary of earth sciences* (3th ed.). Oxford: Oxford University Press.

ASTM C131. (2006). *Standard test method for resistance to degradation of small-size coarse aggregate by abrasion and impact in the Los Angeles machine.* ASTM International, West Conshohocken, PA.

ASTM D7012. (2014). *Standard test methods for compressive strength and elastic moduli of intact rock core specimens under varying states of stress and temperatures.* ASTM International, West Conshohocken, PA.

ASTM C535. (2016). *Standard test method for resistance to degradation of large-size coarse aggregate by abrasion and impact in the Los Angeles machine*. ASTM International, West Conshohocken, PA.

ASTM D4767. (2020a). *Standard test method for consolidated undrained triaxial compression test for soil.* ASTM International, West Conshohocken, PA.

ASTM D7181. (2020b). *Standard test method for consolidated drained triaxial compression test for soil.* ASTM International, West Conshohocken, PA.

Barton, N., & Kjaernsli, B. (1981). Shear strength of rockfill. *Journal of the Geotechnical Engineering Division*, 107(7), 873-891. http://doi.org/10.1061/AJGEB6.0001167.

Blodgett, J.C. (1986). *Rock riprap design for protection of stream channels near highway structures. Volume 1: hydraulic characteristics of open channels* (Water-Resources Investigation Report, No. 86-4127). Reston: USGS.

Coulomb, C.A. (1776). Essai sur une application des règles de Maximis et Minimis à quelques Problèmes de Statique, relatifs à l'Architecture. *Mémoires de l'Académie Royale des Sciences*, 7, 343-382.

Cruz, P.T., & Nieble, C.M. (1970). *Engineering properties of residual soils and granular rocks originated from basalts – Capivara Dam – Brazil.* São Paulo: IPT.

Cruz, P.T., Materón, B. & Freitas, M. (2014). *Barragem de enrocamento com face de concreto.* São Paulo: Oficina de Textos.

DNIT 141. (2012). *Pavimentação: base estabilizada granulometricamente: especificação de serviço.* Departamento Nacional de Infraestrutura de Transportes, Brasília,

Duncan, J.M., & Chang, C. (1970). Nonlinear analysis of stress and strain in soils. *Journal of the Soil Mechanics and Foundations Division*, 96(5), 1629-1652. http://doi.org/10.1061/JSFEAQ.0001458.

Fracassi, G. (2017). *Proteção de rios com soluções Maccaferri.* São Paulo: Oficina de Textos.

Frascá, M.H.B.O. (2019). Assessment of alterability of basalt used for riprap by petrographic examination. *Journal of Rock Mechanics and Geotechnical Engineering*, 11(1), 208-213. http://doi.org/10.1016/j.jrmge.2018.06.009.

Kondner, R.L. (1963). Hyperbolic stress-strain response: cohesive soils. *Journal of the Soils Mechanics and Foundations Division*, 89(1), 115-143.

Kondner, R.L., & Horner, J.M. (1965). Triaxial compression of a cohesive soil with effective octahedral normal stress control. *Canadian Geotechnical Journal*, 2(1), 40-52. http://doi.org/10.1139/t65-004.

Kondner, R.L., & Zelasko, J.S. (1963). Hyperbolic stress-strain formulation for sands. In *Proceedings of the 2nd Pan American Conference on Soil Mechanics and Foundation Engineering* (pp. 289-324), São Paulo.

Leps, T.M. (1970). Review of shearing strength of rockfill. *Journal of the Soil Mechanics and Foundations Division*, 964, 1159-1170. http://doi.org/10.1061/JSFEAQ.0001433.

Maynord, S.T., Ruff, J.F., & Abt, S.R. (1989). Riprap design. *Journal of Hydraulic Engineering*, 115(7), 937-949. http://doi.org/10.1061/(ASCE)0733-9429(1989)115:7(937).

Midea, N.F. (1973). *Ensaio de cisalhamento direto (em laboratório) sobre enrocamento de gnaisse: obra Paraibuna* (Relatório G-07/73). LEC/CESP.

Pichler, E. (1942). *A petrologia e os ensaios tecnológicos de rochas* (Boletim do DER). São Paulo: Departamento de Estradas de Rodagem.

Rawee, L.M., Mohamed, A.I., & Kheder, M.E. (2022). Suitability of sandstone rocks as cladding stones (Riprap) for riverbank protection, from Injana formation, Northern Iraq. *IOP Conference Series: Earth and Environmental Science*, 1080, 012005. http://doi.org/10.1088/1755-1315/1080/1/012005.

Sandroni, S.S. & Guidicini, G. (2021). *Barragens de terra e enrocamento.* São Paulo: Oficina de Textos.

Sayão, A.S.F.J., Maia, P.C.A., & Nunes, A.L.L.S. (2005). Considerations on the shear strength behavior of weathered rockfill. In *Proceedings 16th International Conference on Soil Mechanics and Geotechnical Engineering* (pp. 1917-1920). Millpress Science. http://doi.org/10.3233/978-1-61499-656-9-1917.

Sherard, J.L., Woodward, R.J., Gizienski, S.F., & Clevenger, W.A. (1963). *Earth and earth-rock dams*. New York: John Wiley & Sons.

Terzaghi, K.V. (1960). Closure to “Rockfill Dams: Wishon and Courtright Concrete Face Dams”. *Journal of the Power Division*, 86(part II), 89-92.

United States Department of Agriculture – USDA. Soil Conservation Service. (1989). L*oose riprap protection*. St. Paul: USDA.

Vick, S. (1990). *Planning, design, and analysis of tailings dams*. Vancouver: Bitech.

Yoshida, R. (1972). *Contribuição ao conhecimento das características tecnológicas dos materiais rochosos* [Doctoral thesis]. São Paulo: Universidade de São Paulo.